Appl. Magn. Reson. 31, 193–204 (2007)

Applied Magnetic Resonance

Magnetic Field Dependence of ^{13}C Photo-CIDNP MAS NMR in Plant Photosystems I and II

E. Roy[1], A. Diller[1], Alia[1], P. Gast[2], H. J. van Gorkom[2], H. J. M. de Groot[1], G. Jeschke[3], and J. Matysik[1]

[1] Leiden Institute of Chemistry, Gorlaeus Laboratory, Leiden, The Netherlands
[2] Leiden Institute of Physics, Huygens Laboratory, Leiden, The Netherlands
[3] Fachbereich Chemie, Universität Konstanz, Konstanz, Germany

Received August 19, 2006; revised September 6, 2006

Abstract. Photochemically induced dynamic nuclear polarization is observed in the two photosynthetic reaction centers of plants, photosystem I (PSI) and photosystem II (PSII) by ^{13}C magic-angle spinning nuclear magnetic resonance (NMR) at three different magnetic fields 17.6, 9.4, and 4.7 T. There is a significant difference in field dependence detected in the light-induced signal pattern of the two photosystems. For PSII the optimal NMR enhancement factor of about 5000 is observed at 4.7 T. On the other hand, the maximal light-induced signals of PSI are observed at 9.4 T.

1 Introduction

Photosynthesis in plants involves the participation of two reaction centers (RCs), photosystem I (PSI) and photosystem II (PSII), located in the thylakoid membrane of chloroplasts. These two photosystems belong to two different classes of RCs, namely, type I and type II. The electron transfer chain of both types of photosystems has two symmetric branches consisting of six chlorine molecules and two quinones. PSI belongs to type I RCs, characterized by three iron-sulfur [4Fe-3S] clusters as terminal intrinsic electron acceptors, while PSII belongs to the type II RCs, where a mobile quinone acts as terminal electron acceptor. The primary donors of both RCs differ in their redox potential by about 700 mV [1]. The oxidized primary electron donor of PSII, $P680^{\bullet+}$ is the strongest oxidizing agent known in living nature, having a redox potential of 1.2 V [2]. On the other hand, the electronically excited primary electron donor of PSI, $P700^{*}$, is probably the most reducing compound in living nature [3]. The coupling of these two photosystems allows for pumping electrons across the photosynthetic membrane from water molecules finally into CO_2 in

order to build up organic material. Despite their opposite functional roles, structural similarities in the arrangement of transmembrane helices in the cores of the two photosystems have been observed by recent structural data on PSI [4] and PSII [5].

Photochemically induced dynamic polarization (photo-CIDNP) is well known in liquid nuclear magnetic resonance (NMR) [6–8] as a method that increases NMR intensities. Strongly enhanced signals of solid samples under illumination with continuous white light have been observed for the first time by applying ^{15}N magic-angle spinning (MAS) NMR to quinone-blocked bacterial RCs of *Rhodobacter sphaeroides* R26 [9, 10]. ^{13}C photo-CIDNP MAS NMR experiments of R26 [11–14] and wild type (WT) [15–17] allow one to study the photochemically active regions in great detail. Furthermore, photo-CIDNP has also been observed in both plant RCs. The ^{13}C photo-CIDNP MAS NMR signals obtained from the D1D2 complex of PSII provide evidence of a highly asymmetric electron spin density shifted towards C-15 methine bridge on the donor chlorophyll (Chl) [18]. The ^{13}C photo-CIDNP MAS NMR data of the PSI complex show that all signals are emissive and can be assigned to a single Chl *a* molecule of the primary donor P700 [19]. Comparison between the two photosystems reveals that P700 is essentially an undisturbed Chl *a* cofactor, while the electronic structure of the P680 can be interpreted in terms of a monomeric Chl *a* cofactor having strong matrix interaction [20].

The exact mechanism of photo-CIDNP has recently been discussed [14, 17, 21]. In RCs of *R. sphaeroides* WT, photo-CIDNP has been explained as combination of two parallel mechanisms [17]. The electron–electron–nuclear three-spin mixing (TSM) [22] is related to the coupling between two electron spins in a radical pair state, leading to enhanced polarization of the radical ions. This electron polarization is then transferred by an anisotropic hyperfine coupling to polarization of nuclear spins. The differential decay (DD) [23] mechanism also requires anisotropic hyperfine coupling, but the transfer of the pair polarization to single radical ion polarization arises from superposition of the singlet and triplet state of the radical pair and subsequent preferential decay of pairs in the triplet states. On the other hand, in RCs of *R. sphaeroides* R26, the caroteneless mutant, having a long lifetime of the donor triplet state, a third mechanism is involved [14]. This differential relaxation mechanism (DR) is based on partial extinguishing of nuclear polarization on the triplet branch, while the nuclear polarization of the singlet branch survives entirely [24]. These interpretations are in line with the magnetic field effects observed, showing NMR enhancement maxima of about 10000 at 4.7 T in both bacterial RCs [14, 17]. Hence, magnetic field dependence of photo-CIDNP signals is a sensitive tool to study photo-CIDNP mechanisms and the linked magnetic parameters. Here we present field-dependent ^{13}C photo-CIDNP MAS NMR data of plant PSI and PSII.

2 Materials and Methods

2.1 Preparation of PSI and PSII Reaction Centers

From spinach (*Spinacia oleracea*), the PSI complex containing about 110 Chl/P700 was prepared according to the method described in ref. 19 and the PSII RC (D1D2-cytb559) was prepared according to the method described in ref. 18.

2.2 MAS NMR Measurements

The NMR experiments were performed using DSX-750, DMX-400 and DMX-200 NMR spectrometers (Bruker GmbH, Karlsruhe, Germany). The samples were loaded into optically transparent 4 mm sapphire rotors. The PSI sample was reduced by the addition of an aqueous solution of 10 mM sodium dithionite and 40 mM glycine buffer (pH 9.5) in an oxygen-free atmosphere. Immediately following the reduction, slow freezing of the sample was performed directly in the NMR probe inside the magnet with liquid-nitrogen-cooled gas under continuous illumination with white light. The PSII sample was also frozen slowly directly in the NMR probe inside the magnet with liquid-nitrogen-cooled gas. Temperature has been 223 K, except for experiments at 400 MHz, which were performed at 240 K. The illumination setup was specially designed for the Bruker MAS probe [12]. The light and dark spectra were obtained with a Hahn echo pulse sequence and two-pulse phase modulation (TPPM) proton decoupling [25]. Artificial line broadening of 30 (at 4.7 T), 70 (9.4 T) and 120 Hz (17.6 T) has been applied. The number of scans was 20 k, unless stated differently.

2.3 Calculations

Numerical simulations of the field dependence of photo-CIDNP effects for PSI were based on the theory described in ref. 21 as implemented in a home-written Matlab program for density matrix computation using the EasySpin library [26]. The program starts from a pure singlet state of the pair and computes time evolution under a Hamiltonian including electron Zeeman, nuclear Zeeman, and hyperfine interaction as well as dipole–dipole and exchange coupling between the two electron spins. The part of the density matrix that decays to the ground state from either singlet or triplet radical pairs is projected out (diamagnetic part) and is further evolved under a Hamiltonian including only the nuclear Zeeman interaction. Evolution is computed for a total time that exceeds the lifetime of both singlet and triplet pairs by a factor of five, so that radical pairs have completely decayed. At that time, nuclear polarization of the diamagnetic part of the density matrix is determined. As an extension to the approach described in ref. 21, this procedure is performed for a full powder average [17], describing all interactions by tensors, except for the nuclear Zeeman interaction, whose anisotropy is negligible on a time scale of 100 ns. A spherical grid (EasySpin func-

tion *sphgrid*) with 16 knots and C_i symmetry (481 orientations) was found to be sufficient for powder averaging. Nuclear polarization was normalized to the thermal polarization at the measurement temperature of 223 K and the given field.

Only few of the required spin Hamiltonian parameters for PSI RCs are known from experiments. The principal values for the *g*-tensor of the primary donor cation radical, 2.00304, 2.00262, and 2.00220 were taken from ref. 27. To the best of our knowledge, no high-field EPR measurements of the *g*-tensor have been reported for the primary acceptor in PSI, which is believed to be a Chl *a* [28], nor for the Chl *a* anion radical. To obtain this missing *g*-tensor, the orientations of the principal axes of both *g*-tensors, and the ^{13}C hyperfine couplings, we have performed density functional theory (DFT) computations based on the reported crystal structure of cyanobacterial PSI [28]. From the protein database (PDB) structure 1JB0 we extracted the Chl molecules CL2 1011 and CL11021 as the P700 donor and the Chl molecule CL1 1013 as the putative primary acceptor. The amino acid residues that coordinate the Mg atoms of the Chl molecules were also extracted, His A680 and His B660 for the P700 donor and Met A688 for the acceptor. For the DFT computations, histidines were edited to methylimidazole molecules and methionine was edited to ethyl methyl thioether, and the phytyl chains of the Chl molecules were replaced by methyl groups. Hydrogen atoms were added with the program Titan (Wavefunction, Inc., Irvine, CA, USA). In this procedure some sp^3 carbons were wrongly assigned as sp^2 carbons – these were edited by hand to sp^3 in the same program.

DFT computations were performed with the program ADF 2004.1 using the BLYP functional [29]. The geometry of the P700 donor cation radical was optimized, using a double-zeta basis set (DZ) and frozen cores up to 1s for C, N, and O atoms and up to 2p for the Mg atom. The *g*-tensor was computed by a spin-restricted spin–orbit relativistic computation within the zeroth-order relativistic approximation (ZORA) approach, using all-electron DZ basis sets for all atoms. Hyperfine couplings were obtained from a spin-unrestricted nonrelativistic computation also using all-electron DZ basis sets. In attempts to optimize the geometry of the acceptor anion radical, we found that the distance between the Mg atom of the Chl and the coordinated S atom of the ethyl methyl thioester, which is 0.26 nm in the crystal structure [28], increased continuously. This may indicate that the unusual sulfur coordination to the magnesium is imposed by the structure of the protein and serves for fine-tuning the electron transfer chain, possibly by influencing the redox potential of the primary acceptor. For DFT computations of magnetic parameters, we used the geometry as derived from the crystal structure without further optimization. The *g*-tensor of the acceptor anion radical was computed in the same way as for the P700 donor cation radical. Whereas the principal axes directions were directly taken from the computation, the deviations of the principal values from the free electron *g* value were scaled by a factor *F* that gave the best agreement between experimental principal values and rescaled computed values for the bacteriopheophytin acceptor in bacterial RCs. We consider the principal values obtained by this procedure for the PSI acceptor (2.0039, 2.0030, 2.0024) as rough estimates. For the purpose of the present work they are nevertheless sufficient, as

is discussed below. Hyperfine couplings for the acceptor were obtained from a spin-unrestricted nonrelativistic computation using all-electron TZ2P basis sets for all atoms.

The remaining parameters in the spin Hamiltonian (exchange coupling and dipole–dipole coupling between the two electron spins) and in radical pair kinetics (recombination rates of singlet and triplet radical pairs) have not been determined exactly. However, the geometry and general electronic structure of the relevant part of the PSI RC is quite similar to bacterial RCs, so that we assume that the dipole–dipole coupling between the electron spins is rather close to the value determined on bacterial RCs [30]. The average lifetime of the $P700^+$-A_0^- RC of about 40 ns at zero magnetic field [31] constrains the lifetimes of singlet and triplet pairs. These lifetimes, as well as the exchange coupling between the electron spins, were varied in our photo-CIDNP simulations as described below.

3 Results and Discussion

3.1 Field Effects in the Dark Spectra

Figure 1 shows the ^{13}C MAS NMR spectra of PSI samples at three different magnetic fields at 17.6 T (750 MHz proton frequency), 9.4 T (400 MHz) and 4.7 T (200 MHz). All spectra are recorded at a MAS rotational frequency of 8 kHz. In none of the spectra any significant signal of the protein backbone appears. This is due to the presence of a low amount of protein, 0.6 mg, present in the rotor. The signals observed at 42 and 175 ppm probably arise from glycine used as cryoprotectant in the buffer. However, the signals are weak at 4.7

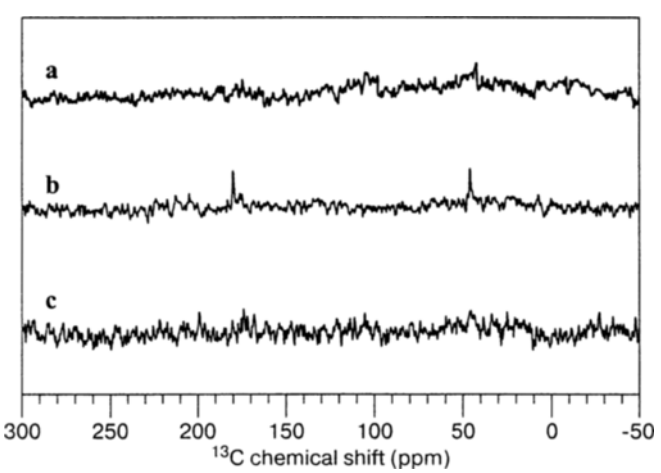

Fig. 1. ^{13}C MAS NMR spectra of PSI particles obtained in the dark with a MAS frequency of 8 kHz at 17.6 (**a**), 9.4 (**b**), and 4.7 (**c**) T.

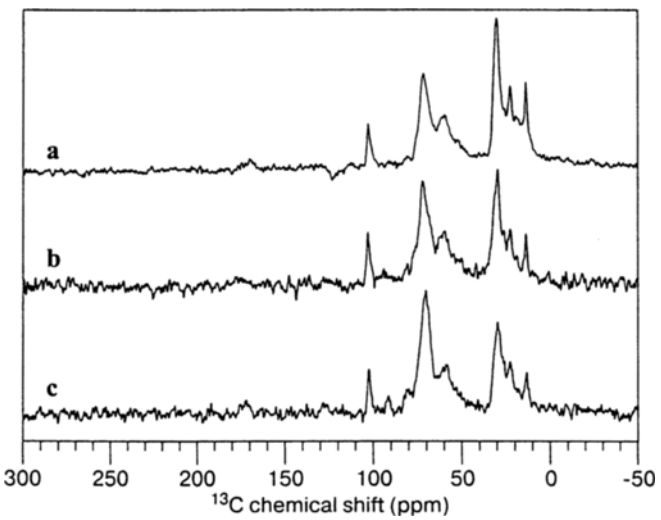

Fig. 2. ^{13}C MAS NMR spectra of PSII (D1D2) particles obtained in the dark with a MAS frequency of 8 kHz at 17.6 (**a**), 9.4 (**b**), and 4.7 (**c**) T.

T, while at 17.6 T they could not be detected, probably due to the lower number of scans.

Figure 2 shows the spectra of PSII particles at the same condition. The amount of protein in the rotor has been determined to be 15.8 mg. All three dark spectra show similar features. All signals appear between 110 and 10 ppm, except for weak features in the aromatic and carbonylic region. The signals arise from the protein and the BTS-200 buffer. The spectra are typical ^{13}C MAS NMR spectra of large proteins [32]. No spinning sidebands are observed in the three spectra. This is due to the small chemical shift anisotropy (CSA) of aliphatic carbons and the small signal intensity of the carbonylic and aromatic signals. The spectral quality obtained at 17.6 T is slightly above that obtained at 9.4 T. The spectra obtained at 17.6 and 9.4 T are clearly better resolved than that obtained at 4.7 T. The observed field dependence is due to lower Zeeman spitting and chemical shift dispersion at lower fields under Boltzmann conditions.

3.2 Field Effects in the Light Spectra

Upon illumination with continuous white light, strong signals emerge in the aromatic region in both PSI (Fig. 3) and in PSII (Fig. 4). In PSI, all light-induced signals appear to be emissive (negative) [19] between 170 and 80 ppm. In the spectrum at 17.6 T (Fig. 3a), spinning sidebands can be observed, whereas at lower fields the entire intensity is concentrated in the centerband. The strongest signals are observed at 9.4 T (Fig. 3b), while the weakest signals are observed at 4.7 T (Fig. 3c). Figure 5a expresses the field dependence of the light-induced

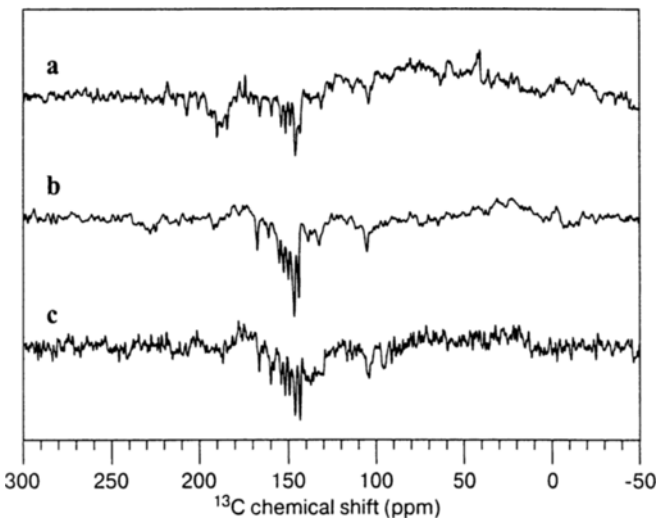

Fig. 3. ^{13}C MAS NMR spectra of PSI particles obtained under continuous illumination with white light at a MAS frequency of 8 kHz at 17.6 (**a**), 9.4 (**b**), and 4.7 (**c**) T.

centerband signals relative to the noise standardized to a single scan. Figure 5a shows a clear maximum at 9.4 T and about half intensity at 17.6 T. Absence of reliable dark signals does not allow for calculation of absolute enhancement factors in PSI.

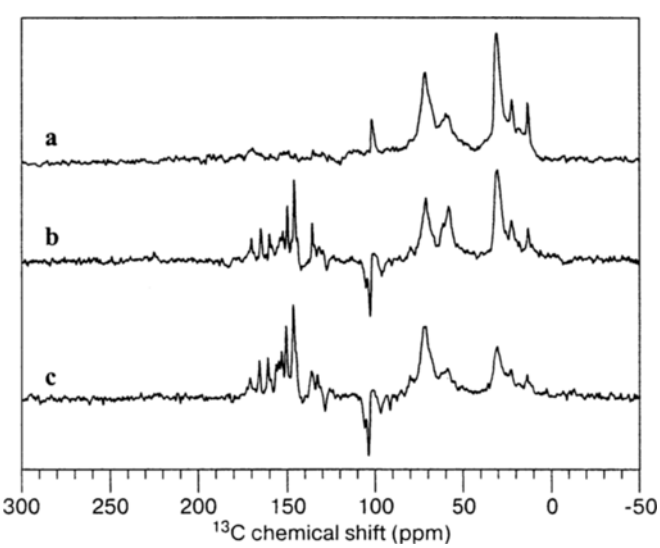

Fig. 4. ^{13}C MAS NMR spectra of PSII (D1D2) particles obtained under continuous illumination with white light at a MAS frequency of 8 kHz at 17.6 (**a**), 9.4 (**b**), and 4.7 (**c**) T.

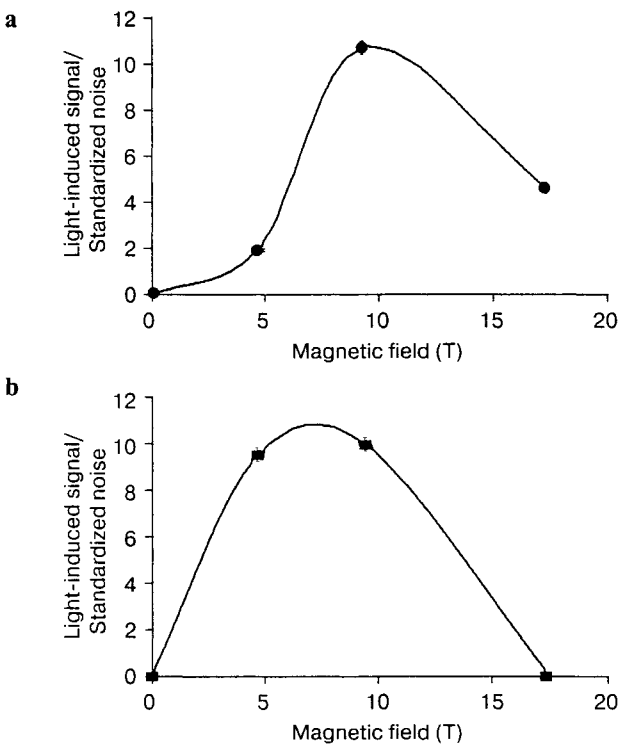

Fig. 5. **a** Field dependence of the light-induced signal to the standardized noise for PSI. **b** Field-dependence of the light-induced signal to the standardized noise for PSII.

In PSII, strong enhancement is observed at 4.7 and 9.4 T (Fig. 4b and c), while at 17.6 T (Fig. 4a) no light-induced signals are observed. Comparing Fig. 4b and c indicates slightly stronger enhancement compared to the dark signals at 4.7 T. In contrast to the light-induced signals in PSI, both enhanced absorptive and emissive light-induced signals occur. The emissive signals mainly appear in the region of the methine carbons. In the spectrum at 9.4 T, slight spinning sidebands occur. Using the signal from about 900 methyl groups of the entire D1D2 complex at 13.7 ppm as internal standard, enhancement factors of ≤ 60 (17.6 T), 3000 (9.4 T) and about 5000 (4.7 T) were calculated for PSII (Fig. 6). The field dependence of the enhancement factor of PSII is similar to that observed in bacterial RCs of both WT and R26 [14, 17], showing a maximum at 4.7 T and a strong decay at higher fields. The field dependence of the light-induced signal to the standardized noise is shown in Fig. 5b, allowing for comparison with PSI (Fig. 5a), suggesting a shift of optimum photo-CIDNP production in PSI to higher fields.

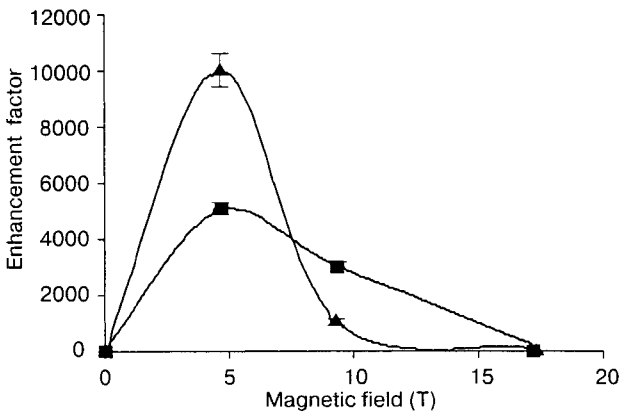

Fig. 6. Enhancement factors at different magnetic fields calculated for PSII (■) along with R26 (▲).

3.3 Simulations of Field Effects in Light Spectra of PSI

The field dependence of the photo-CIDNP effects in PSII is similar to previous observations on bacterial RCs, with maximum polarization at the lowest tested field of 4.7 T (Fig. 6). In contrast, PSI exhibits only a relatively weak photo-CIDNP effect at 4.7 T and a much stronger polarization at 9.4 T (Figs. 3 and 5a). As the field dependence of the nuclear polarization is related to the magnetic parameters and lifetimes of the intermediate radical species [17, 21], this difference must be related to a difference in the electronic structure between RCs of purple bacteria and PSII on the one hand and PSI RCs on the other hand.

To examine what parameter changes can explain the experimental observations, we have performed simulations of the photo-CIDNP in an analogous manner as the simulations of bacterial RCs, which reproduced the experimental field dependence [17]. Generally, we find that the field dependence of the nuclear polarization is similar for all ^{13}C nuclei in both donor and acceptor molecules, as was also found for the bacterial RCs. This simulation result agrees with the experimental observation that the spectral pattern varies only slightly between 4.7 and 17.6 T (Fig. 3). Furthermore, we find that any reasonable changes in the *g*-tensors (up to $\pm 50\%$ of the deviation from the free electron *g*-value) cause only a scaling of the intensity of the whole spectral pattern by a constant factor, which does not depend significantly on magnetic field. In other words, uncertainties in the computation of the acceptor *g*-tensor and of the principal axes directions of the *g*-tensors do not lead to significant uncertainties in the computed field dependence of the nuclear polarization. Likewise, any reasonable changes in the dipole–dipole coupling (up to $\pm 30\%$ of the coupling strength) have no significant influence on the field dependence. The pronounced difference between bacterial and PSII RCs on the one hand and PSI RCs on the other hand can thus be traced back to either a difference in radical pair lifetimes or a difference in the exchange coupling *J*.

Assuming the same J and lifetimes as for bacterial RCs, we find a very similar field dependence of the nuclear polarization with a maximum close to 5 T. As an example, the dependence for the methine carbon C-20 of the donor for these assumptions is shown in Fig. 7a. We first tested whether the different field dependence that is observed for PSI RCs can be reproduced by changing the ratio between the lifetime T_S of radical pairs in the singlet state and the lifetime T_T of radical pairs in the triplet state. However, changes in the field dependence of the nuclear polarization are minor when varying the ratio T_S/T_T between 0.5 and 50 (data not shown).

Next, we tested whether changes in the mean lifetime of radical pairs, defined here as $\sqrt{T_S T_T}$, can reproduce the observations. Indeed the shift of the maximum to a field of approximately 8.5 T can be obtained by decreasing $\sqrt{T_S T_T}$ to 1.6 ns (data not shown). This value cannot directly be compared to the experimental lifetime, as the combination of the lifetimes T_S and T_T to the true mean lifetime depends on the specifics of spin evolution and would have to be computed by including hyperfine coupled protons in the spin Hamiltonian. However, the mean lifetime cannot be larger than the maximum of T_S and T_T,

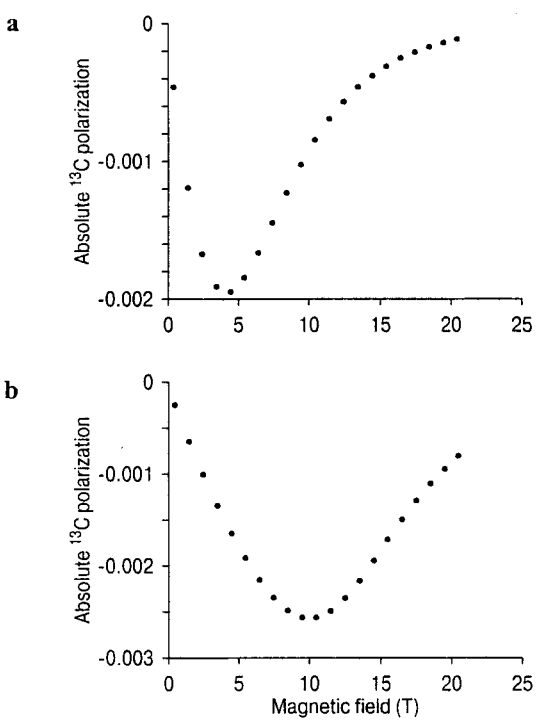

Fig. 7. Simulated field dependence of the absolute ^{13}C polarization for donor methine carbon C-20 of the active branch of the P700 donor. Similar results are obtained for other carbon atoms in both donor and acceptor. **a** RC lifetimes and exchange coupling as in bacterial RCs. **b** RC lifetime as in bacterial RCs, but exchange coupling increased by a factor of 3.

which is 5 ns for simulations that fit the observed field dependence. It seems unlikely that the RC lifetime in our samples is by almost a factor of 10 shorter than found on cyanobacterial PSI [31]. Even if we would assume that, we would still be left with the fact that such a shortening of the lifetime leads to a drastic decrease in the absolute nuclear polarization, which does not agree with the similar NMR sensitivity observed in photo-CIDNP experiments on bacterial RCs and plant PSI RCs. We thus exclude a shortening of the RC lifetime as the cause for the change in the field dependence.

Finally, we considered variations of the exchange coupling J. An increase of the exchange coupling by a factor of three compared to bacterial RCs to 21 G shifts the field where maximum nuclear polarization is attained to about 10 T (Fig. 7b). This leads to a slight increase in absolute polarization, which can be reconciled with experimental observations. Such a change in J may well be caused by slight rearrangements of the cofactors that lead to an improved overlap between the molecular orbitals of the P700 donor and the accessory Chl *a* or between the molecular orbitals of the accessory Chl and the primary acceptor A_0. The simulations thus indicate that the change in the magnetic field dependence of solid-state photo-CIDNP between bacterial RCs and plant PSI can be traced back to an increase of the exchange coupling between the $P700^+$ and A_0^- radical anions by a factor of approximately 3. The underlying cause for this change is the influence of a large exchange coupling on the matching condition [21]. In the limit where the exchange coupling is much larger than the hyperfine couplings and the difference of the electron Zeeman frequencies, state mixing is optimum when the coupling between the electron spins matches the nuclear Zeeman frequency. In the limit of large exchange couplings, the optimum magnetic field is thus proportional to the exchange coupling.

Acknowledgments

The help of F. Lefeber, J.G. Hollander and K. Erkelens is gratefully acknowledged. This work has been financially supported by the Netherlands Organization for Scientific Research (NWO) through Jonge Chemici award (700.50.521), an open-competition grant (700.50.004) and a Vidi grant (700.53.423) as well as by the Volkswagen-Stiftung (I/78010) to J.M.

References

1. Grotjohann I., Jolley C., Fromme P.: Phys. Chem. Chem. Phys. **6**, 4743–4753 (2004)
2. van Gorkom H.J., Schelvis J.P.M.: Photosynth. Res. **38**, 297–301 (1993)
3. Webber A.N., Lubitz W.: Biochim. Biophys. Acta **1507**, 61–79 (2001)
4. Jordan P., Fromme P., Witt H.T., Klukas O., Saenger W., Krauss N.: Nature **411**, 909–917 (2001)
5. Zouni A., Witt H.T., Kern J., Fromme P., Krauss N., Saenger W., Orth P.: Nature **409**, 739–743 (2001)
6. Roth H.D. in: Encyclopedia of Nuclear Magnetic Resonance (Grant D.M., Harris R.K., eds.), vol. 2, p. 1337. Chichester: Wiley 1996.

7. Hore P.J., Broadhurst R.W.: Prog. Nucl. Magn. Reson. Spectrosc. **25**, 345–402 (1993)
8. Goez M.: Adv. Photochem.: **23**, 63–164 (1997)
9. Zysmilich M.G., McDermott A.: J. Am. Chem. Soc. **116**, 8362–8363 (1994)
10. Zysmilich M.G., McDermott A.: J. Am. Chem. Soc. **118**, 5867–5873 (1996)
11. Zysmilich M.G., McDermott A.: Proc. Natl. Acad. Sci. USA **93**, 6857–6860 (1996)
12. Matysik J., Alia, Hollander J.G., Egorova-Zachernyuk T., Gast P., de Groot H.J.M.: Indian J. Biochem. Biophys. **37**, 418–423 (2000)
13. Matysik J., Alia, Gast P., Lugtenburg J., Hoff A.J., de Groot H.J.M. in: Perspectives on Solid State NMR in Biology (Kiihne S.R., de Groot H.J.M., eds.), pp. 215–225. Dordrecht: Kluwer Academic 2001.
14. Prakash S., Alia, Gast P., de Groot H.J.M., Matysik J., Jeschke G.: J. Am. Chem. Soc. **128**, 12994–12799 (2006)
15. Schulten E.A.M., Matysik J., Alia, Kiihne S., Raap J., Lugtenburg J., Gast P., Hoff A.J., de Groot H.J.M.: Biochemistry **41**, 8708–8717 (2002)
16. Prakash S., Alia, Gast P., Jeschke G., de Groot H.J.M., Matysik J.: J. Mol. Struct. **661**, 625–633 (2003)
17. Prakash S., Alia, Gast P., de Groot H.J.M., Jeschke G., Matysik J.: J. Am. Chem. Soc. **127**, 14290–14298 (2005)
18. Matysik J., Alia, Gast P., van Gorkom H.J., Hoff A.J., de Groot H.J.M.: Proc. Natl. Acad. Sci. USA **97**, 9865–9870 (2000)
19. Alia, Roy E., Gast P., van Gorkom H.J., de Groot H.J.M., Jeschke G., Matysik J.: J. Am. Chem. Soc. **126**, 12819–12826 (2004)
20. Diller A., Alia, Roy E., Gast P., van Gorkom H.J., Zaanen J., de Groot H.J.M., Glaubitz C., Matysik J.: Photosynth. Res. **84**, 303–308 (2005)
21. Jeschke G., Matysik J.: J. Chem. Phys. **294**, 239–255 (2003)
22. Jeschke G.: J. Chem. Phys. **106**, 10072–10086 (1997)
23. Polenova T., McDermott A.E.: J. Phys. Chem. B **103**, 535–548 (1999)
24. McDermott A., Zysmilich M.G., Polenova T.: Solid State Nucl. Magn. Reson. **11**, 21–47 (1998)
25. Bennett A.E., Rienstra C.M., Auger M., Lakshmi K.V., Griffin R.G.: J. Chem. Phys. **103**, 6951–6958 (1995)
26. Stoll, S., Schweiger A.: J. Magn. Reson. **178**, 42–55 (2006)
27. Petrenko A., Maniero A.L., Van Tol J., MacMillan F., Li Y., Brunel L.-C., Redding K.: Biochemistry **43**, 1781–1786 (2004)
28. Jordan P., Fromme P., Witt H.T., Klukas O., Saenger W., Krauß N.: Nature **411**, 909–917 (2001)
29. Velde G.T., Bickelhaupt F.M., Baerends E.J., Guerra C.F., van Gisbergen S.J.A., Snijders J.G., Ziegler T.: J. Comput. Chem. **22**, 931–967 (2001)
30. Hulsebosch R.J., Borovykh I.V., Paschenko S.V., Gast P., Hoff A.J.: J. Phys. Chem. B **103**, 6815–6823 (1999)
31. Biggins J., Mathis P.: Biochemistry **27**, 1494–1500 (1988)
32. Castellani F., van Rossum B., Diehl A., Schubert M., Rehbein K., Oschkinat H.: Nature **420**, 98–102 (2002)

Authors' address: Jörg Matysik, Leiden Institute of Chemistry, Gorlaeus Laboratory, P.O. Box 9502, 2300 RA Leiden, The Netherlands
E-mail: j.matysik@chem.leidenuniv.nl